Schweizerischer Erdbebendienst
Service Sismologique Suisse
Servizio Sismico Svizzero
Swiss Seismological Service

ETH
Eidgenössische Technische Hochschule Zürich
Swiss Federal Institute of Technology Zurich

# SITE CHARACTERIZATION REPORT

## **SIOH:** Sion Hôpital (VS)

Dario Chieppa, Vincent Perron, Donat Fäh

Last Modification: 18th August, 2022

Schweizerischer Erdbebendienst (SED)
Service Sismologique Suisse
Servizio Sismico Svizzero
Servizi da Terratrembels Svizzer
ETH Zürich
Sonneggstrasse 5
8092 Zürich
Schweiz
dario.chieppa@sed.ethz.ch

# Contents

**Contents** ..... **4**
**1 Introduction** ..... **6**
**2 Geological setting** ..... **7**
**3 Passive site characterization measurements** ..... **8**
**3.1 Data set** ..... 8
**3.2 H/V and RayDec ellipticity curves** ..... 9
**3.3 Polarization measurements** ..... 11
**3.4 3-component high-resolution FK** ..... 11
**3.5 WaveDec** ..... 13
**3.6 Modified SPatial AutoCorrelation** ..... 14
**3.7 Summary** ..... 15
**4 Data inversion** ..... **16**
**4.1 Inversion targets** ..... 16
**4.2 Inversion parameterization** ..... 17
**4.3 Inversion results** ..... 17
**4.4 Discussion of the inversion results** ..... 23
**5 Further results from the inverted profiles** ..... **27**
**5.1 SH transfer function** ..... 27
**5.2 Quarter-wavelength representation** ..... 28
**6 Discussion and conclusions** ..... **29**
**References** ..... **30**

# Summary

Sion (VS) is a city located in southern Switzerland in the middle of Canton Valais. The place was chosen as site for the installation of a new station, called SIOH, as part of the renewal project of the Swiss Strong Motion Network (SSMNet). In order to better assess the local subsurface, we performed a passive seismic array around the location of seismic station SIOH.

The results of the horizontal-to-vertical spectral ratio (H/V) show curves with similar shapes over the entire frequency range. Some variation exists at higher frequencies (above 5 Hz) and are linked with the variability of the shallowest layers. A narrow and sharp peak, interpreted as the fundamental peak ($f_0$), was recognized between 0.45 and 0.49 Hz at all sites. A second and wider peak ($f_1$) was recognized between 5.91 and 8.65 Hz at several sites mostly located in the center of the study area.

The inversion of data collected using the passive seismic array allows the estimation of S-wave velocity profile down to about 800 m. Using a velocity profile with different initial parametrizations, two interfaces are identified in the shallowest 30 meters at about 3 and 15 meters. One or more velocity inversions take place in the first 100 meters in all inverted velocity profiles. Two clusters of models were identified for what concern the half-space: the first cluster presents a strong velocity contrast at about 441-492 m with S-wave velocity up to 3967 m/s; the other shows a gradient going down to 772 m and has S-wave velocity of 3428 m/s.

The average $V_{S30}$ value for the site is 504.55 m/s, corresponding to class B in EC8 and SIA261 classifications. The theoretical shear-wave transfer functions from the estimated $V_S$ profiles predict an amplification function between 0.75 and 3.87 in the frequency range 0.5-11.11 Hz. As of today (16.06.2022), the empirical amplification function for SIOH station has a maximum of 4 events in the frequency range 0.58-7.32 Hz and shows similar shapes with the SH-wave transfer function obtained using the *dinver* velocity models over the frequency range 0.5-7.2 Hz. The SH-wave transfer functions for the *Neopsy* code models, instead, show comparable amplification values but different shapes due to the presence of several sharp peaks.

# 1 Introduction

The station SIOH is part of the Swiss Strong Motion Network (SSMNet). The station was installed on the 8th of September 2021 in the framework of the second phase of the Swiss Strong Motion Network (SSMNet) renewal project (Fig. 1). In order to better characterize the underground, to estimate the fundamental frequency of the site and the shear wave velocity, a passive array measurement was carried out on 28th September 2021.

The site is of interest for its location in a populated area of southern Switzerland, for the possibility to improve the network coverage and for the presence of one of the most important hospital of canton Valais. From a geological point of view, the area around the Sion hospital consists in river gravels and artificial deposits of Holocene age. Gravimetric data (Swisstopo, 2015) located the rock basement at about 400/500 meters.

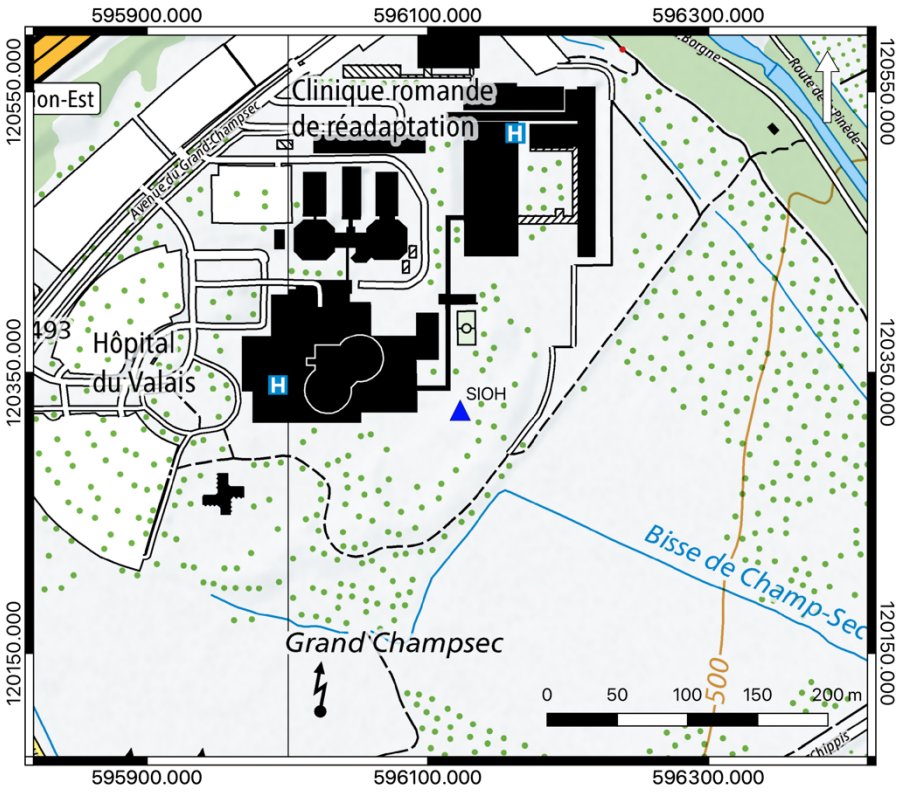


*Figure 1: Map showing the location of the strong motion station (blue triangle) in Sion. Source: Federal Office of Topography.*

# 2 Geological setting

A geological map of the surroundings of Sion hospital is shown in Fig. 2. Red dots represent the locations of the passive array measurement; the blue triangle shows the location of SIOH station. Seven stations were installed on river gravels (Holocene), while the remaining 9 were on artificial deposits (Holocene) or close to the border with the river gravels. The SIOH station is installed at the border between these two geological units.

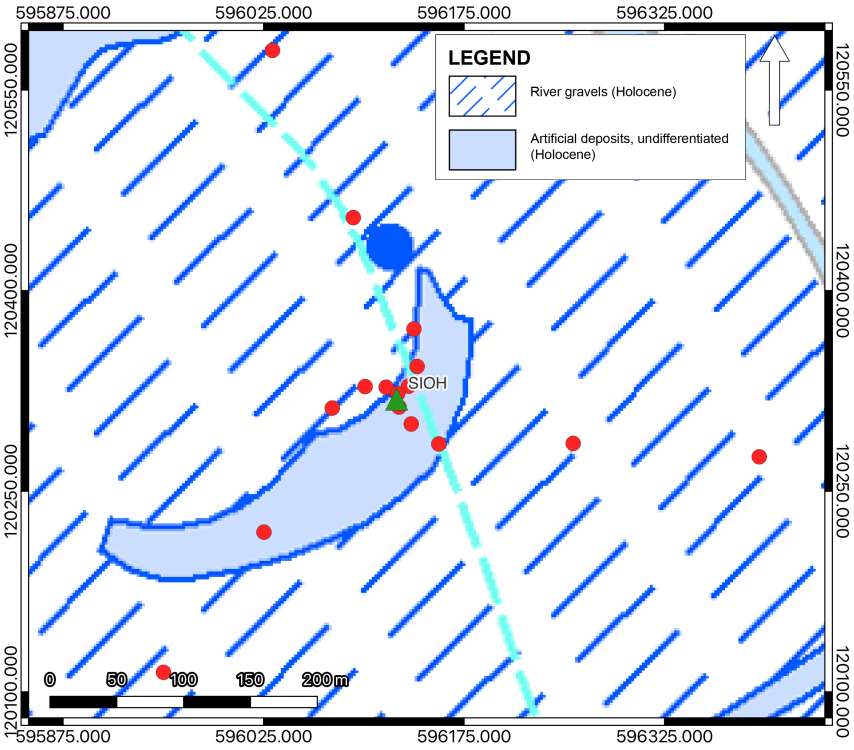


*Figure 2: Geological map of the Sion hospital area. The stations of the passive array recordings are indicated by red triangles, whereas the position of the strong-motion station SIOH is shown by a green triangle. Source: Federal Office of Topography.*

# 3 Passive site characterization measurements

## 3.1 Data set

To characterize the deep underground structure around the seismic station, a passive seismic measurement was performed on 28 September 2021.

A single array of 16 stations was installed (Fig. 3). The stations were planned to be located on five rings of different radii around a central station. The three stations of each ring were planned to be rotated about 120 degrees one from the other. The radii of the rings are 10, 25, 50, 135 and 275 meters. The array central station (SIOH74) is located 3 meters east from the SIOH station. Each ring, starting from the second, was rotated counter-clockwise with respect to the inner ring of 20, 20, 33 and 7 degrees.

Each station consisted of a Lennartz 5s sensor connected to a Centaur digitizer (Fig. 4), with the exception of four stations in the central part where two sensors were connected to the same digitizer. The station names of the array are composed of "SIOH" followed by a two-digit number between 42 and 49, 52 and 55, 65, 72, 74 and 75 (corresponding to the Centaur digitizer serial number for numbers lower than 60 plus 20 to distinguish the use of the second channel). The array recording time was 144 minutes (8640 s). The station locations were measured by a differential GPS system (Leica Viva GS10) which was set up to measure with a precision better than 5.3 cm.

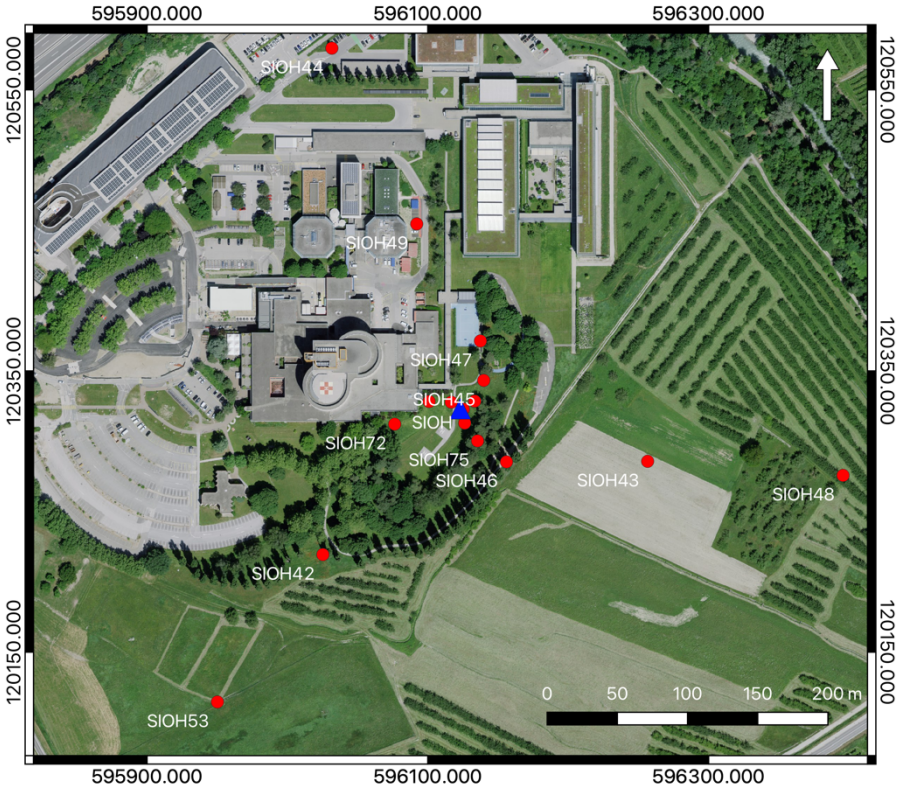


*Figure 3: Layout of the array measurement in Sion. The locations of the stations for the passive seismic measurement are indicated by the red dots. The blue triangle indicates the seismic station site. Source: Federal Office of Topography.*


*Figure 4: Seismic station installation example for the measurements in Sion.*

### 3.2 H/V and RayDec ellipticity curves

In the left plot of Fig. 5, we show the H/V curves determined using Geopsy software (Wathelet et al., 2020) for all stations of the passive array. With the exception of SIOH44 station, located in the north of the study area, all the other H/V curves show a narrow and sharp peak at about 0.43 – 0.44 Hz. Both flanks of the H/V curve are steep: the left flank is short, while the right one is longer and ends in a trough at about 0.84 Hz. To the right of the trough, the H/V curves show an ascending trend ending in a wide peak located between 5.91 and 8.65 Hz. The overall shape of the H/V curves show a study area that it is mostly homogeneous. The effects of shallow heterogeneities can be seen in all H/V curves at frequencies above 5 Hz.

The peak at low frequency is recognized at all sites and is interpreted as the H/V fundamental peak ($f_0$); the other peak, at higher frequencies, is interpreted as secondary peak ($f_1$) and it is mainly visible in the central part of the array and in the southern sector. The areal distribution of the two peaks is shown in Fig. 6.

The RayDec technique (Hobiger et al., 2009) is meant to eliminate the contributions of other wave types than Rayleigh waves and give a better estimate of the ellipticity. The RayDec ellipticity curves for all stations of the array measurements are shown in Figure 5 (right plot). These show a pattern similar to the H/V curves where two peaks can be seen: one narrow and sharp at about 0.44 Hz and the other wide and flat at higher frequencies.

The dark green curve indicates the array central station (SIOH74); the same curve, due to its proximity with the station SIOH, represents the RayDec ellipticity also for the permanent station.

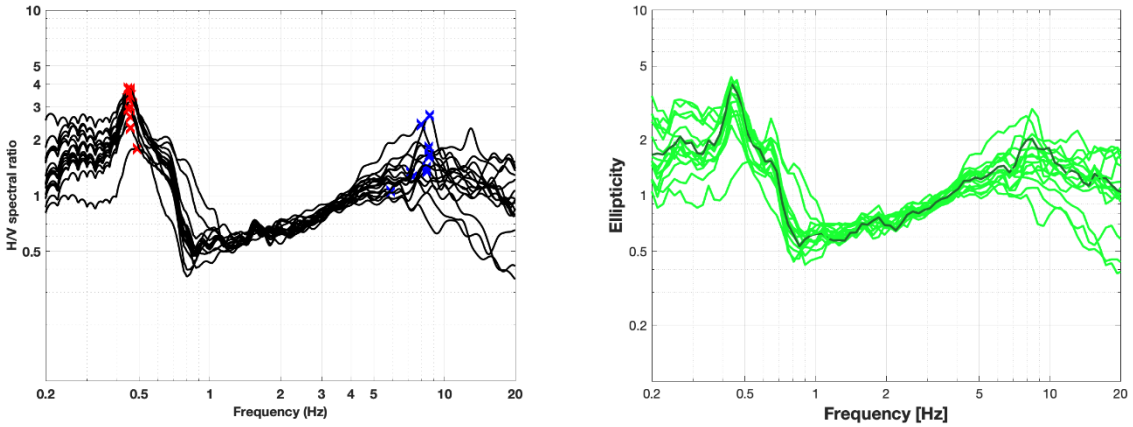


*Figure 5: Left: H/V curves of the different stations of the array measurements in Sion with picked fundamental frequency (red cross). Right: RayDec ellipticities for all stations of the array. The curve of SIOH74, the array center, is highlighted in dark green.*

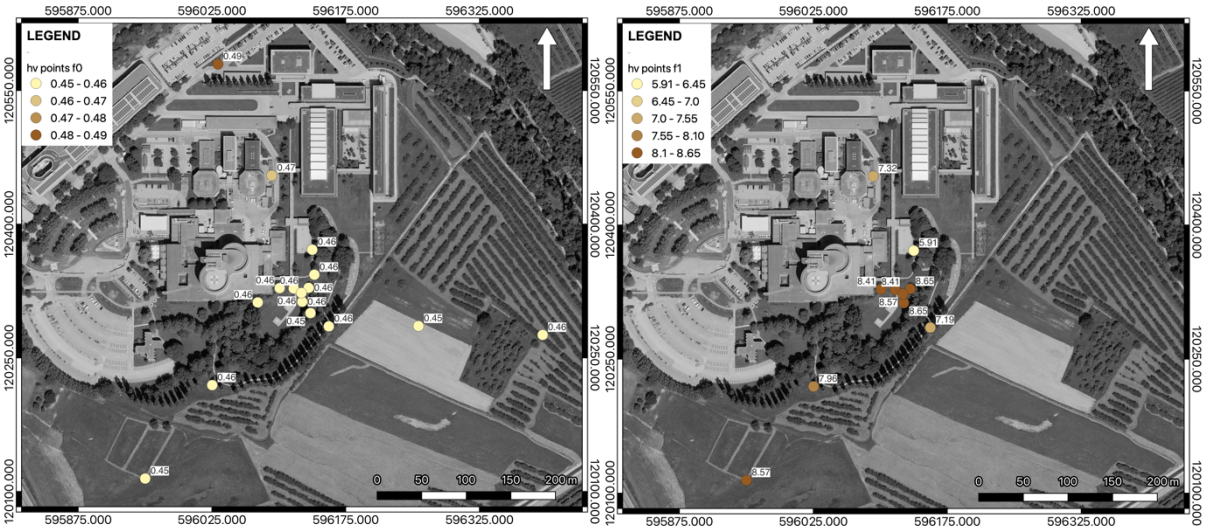


*Figure 6: Map showing the variation in frequency for the H/V fundamental (left) and secondary peak (right) peaks over the area of Sion. Source: Federal Office of Topography.*

### 3.3 Polarization measurements

The polarization analysis was performed according to Burjánek et al. (2010) and Burjánek et al. (2012). The results for all stations of the array are similar. Fig. 7 shows the results for SIOH74, the array central station. The ground motion is quasi-linear polarized around the $f_0$ H/V peak (0.2) changing to quasi-elliptical (0.4) above 0.8 Hz (Fig. 7 – left plot); a weak direction of polarization northeast-southwest oriented can be recognized at the H/V peak (Fig. 7 – right plot) and at all sites of the study area. This direction of polarization shows an angle of 5 degrees with respect to the Rhone valley orientation. The ground motion is quasi-horizontally polarized at about the H/V $f_0$ peak and at 10 Hz (Fig. 7 – central plot).

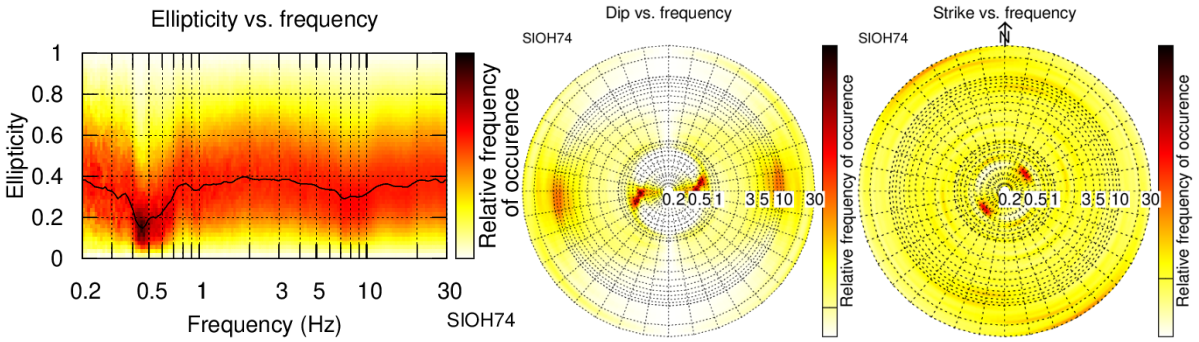


*Figure 7: Polarization analysis of station SIOH74.*

### 3.4 3-component high-resolution FK

The results of the 3-component high-resolution FK analysis (Poggi and Fäh, 2010) are shown in Figs. 8 and 9. For Love waves, using the transverse component, a dispersion curve was picked between 0.96 and 19.84 Hz (Fig. 8 – top row left). The first portion between 0.96 and 3.91 Hz is flat, while the following portion shows a descending trend. The Rayleigh waves were picked using the vertical and the radial components. Two dispersion curves were picked for the vertical component: the first between 0.99 and 22.33 Hz and the second between 6.33 and 11.89 Hz (Fig. 8 – top row right). The first mode shows a short portion with a descending trend up to 1.29 Hz, a long flat portion (1.30 – 9.03 Hz) with S-wave velocities of about 650 m/s and a new change in slope starting at 9 Hz. The second mode is located at higher S-wave velocities and it is mostly straight. Two dispersion curves were picked also for the radial component (Fig. 8 – bottom row); both curves show trends similar to the curves picked for the vertical component. The curve at low velocity is picked between 1.08 and 17.36 Hz, while the other is located between 4.44 and 11.43 Hz. For each curve picked using the vertical and the radial components, the ellipticity curves are picked over the same frequency range. The results are shown in Fig. 9 for the vertical (top row) and radial (bottom row) components; left and right columns show the results for the modes at low and high velocities, respectively. Both curves in the left column show a wide trough and a wide and almost flat peak; right column presents a curves with an ellipticity value of 1/1.5 over the entire frequency range.

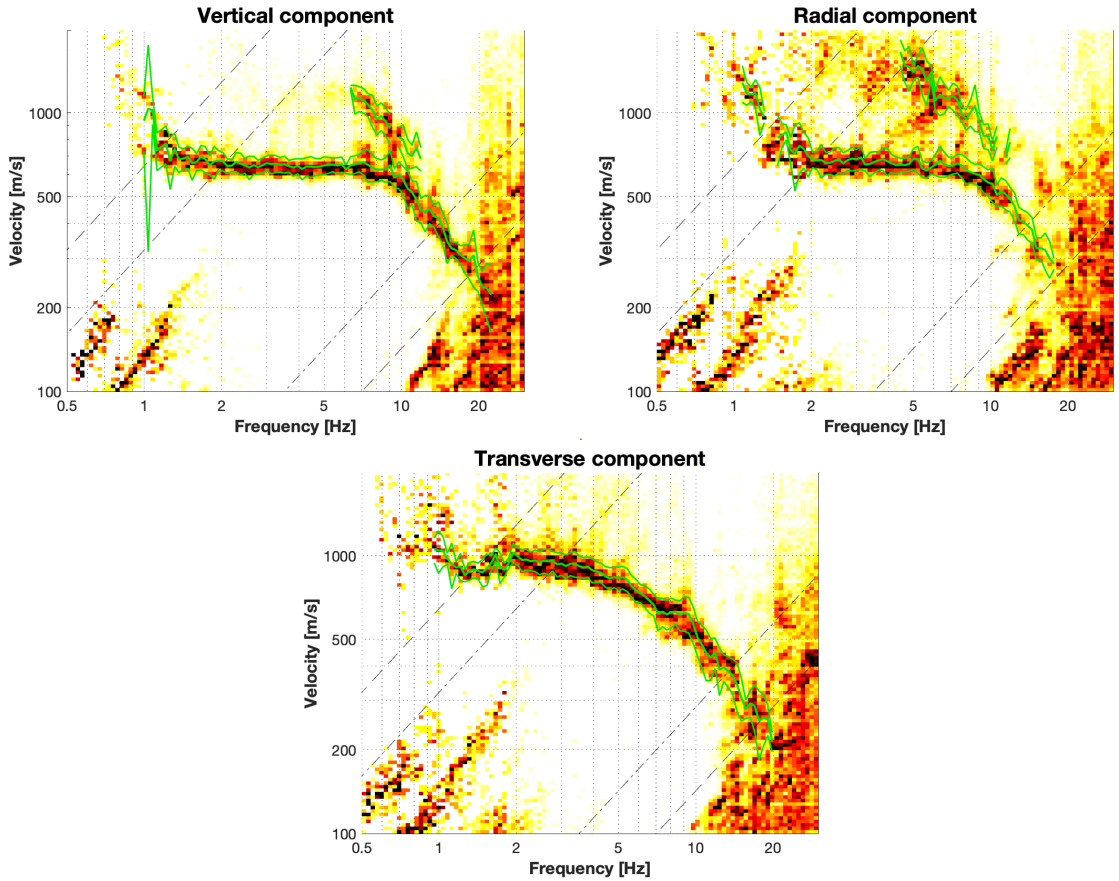


*Figure 8: Dispersion curves for the transverse (top left), vertical (top right) and radial (bottom) components obtained with the 3-component HRFK algorithm (Poggi and Fäh, 2010). The dashed and dotted black lines are the array resolution limits. The solid and dashed green lines represent the data picking (central line) and the standard deviation (outer lines).*

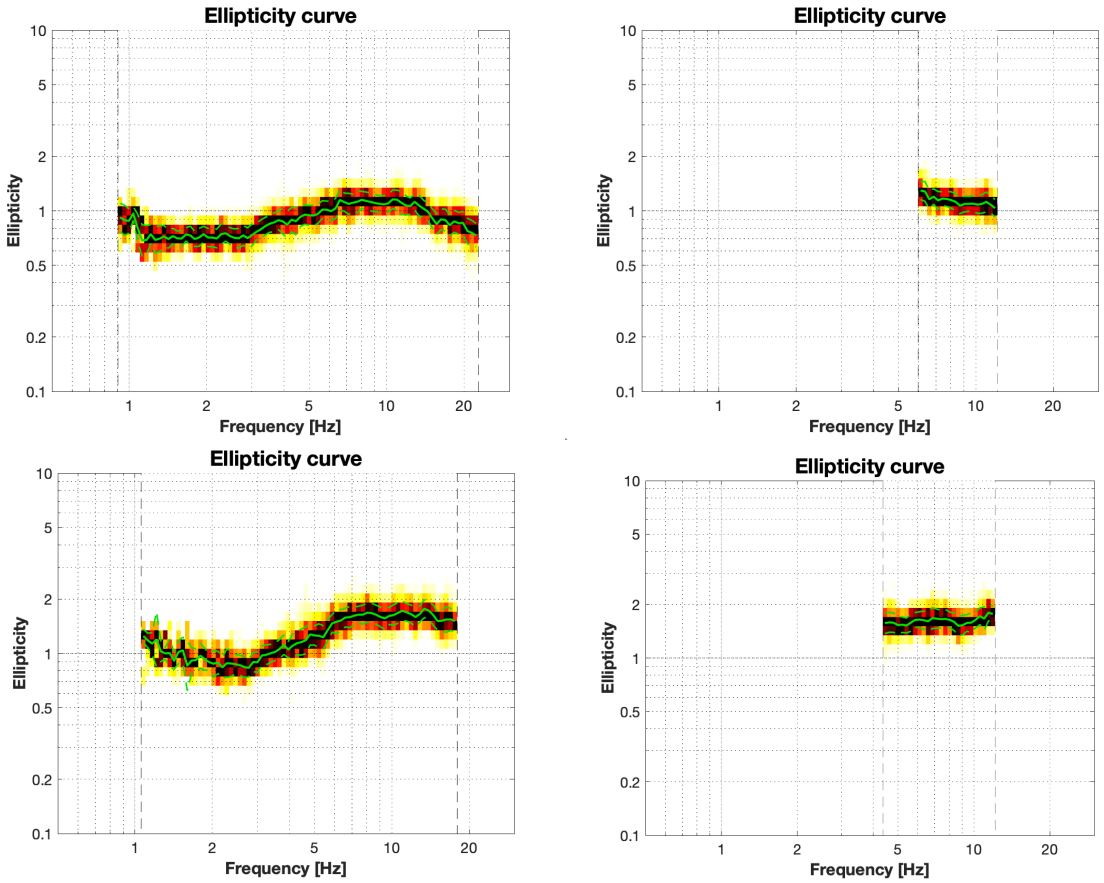


*Figure 9: Ellipticity curves for the vertical (top row) and radial (bottom row) components using the 3-component HRFK algorithm (Poggi and Fäh, 2010). Left column shows the mode picked at lower velocity, while the right column the mode at higher velocities. The dashed vertical lines represent the lower and upper frequencies for the picked dispersion curves. The solid and dashed green lines represent the data picking (central line) and the standard deviation (outer lines).*

## 3.5 WaveDec

The results of the WaveDec (Maranò et al., 2012) processing are shown in Fig. 10. This technique estimates the properties of single or multiple waves simultaneously with a maximum likelihood approach. In order to get good results, the parameter γ must be tuned to modify the sharpness of the wave property estimation between purely maximum likelihood estimation and a Bayesian Information Criterion. Here, a value of $\gamma = 0.1$ was used, corresponding to an almost pure Maximum Likelihood algorithm.

The picking of dispersion curves in WaveDec was performed in the wavenumber-frequency domain. The Love wave dispersion curve was continuously picked between 0.95 and 13.82 Hz. For what concerns the Rayleigh waves, a single dispersion curve was picked between 1.0 and 11.78 Hz. The dispersion curve presents flat between 1.29 and 7.56 Hz and has S-wave velocity of about 600 m/s. The ellipticity angle for the Rayleigh wave dispersion curve is negative over the entire frequency range and its particle motion is retrograde.

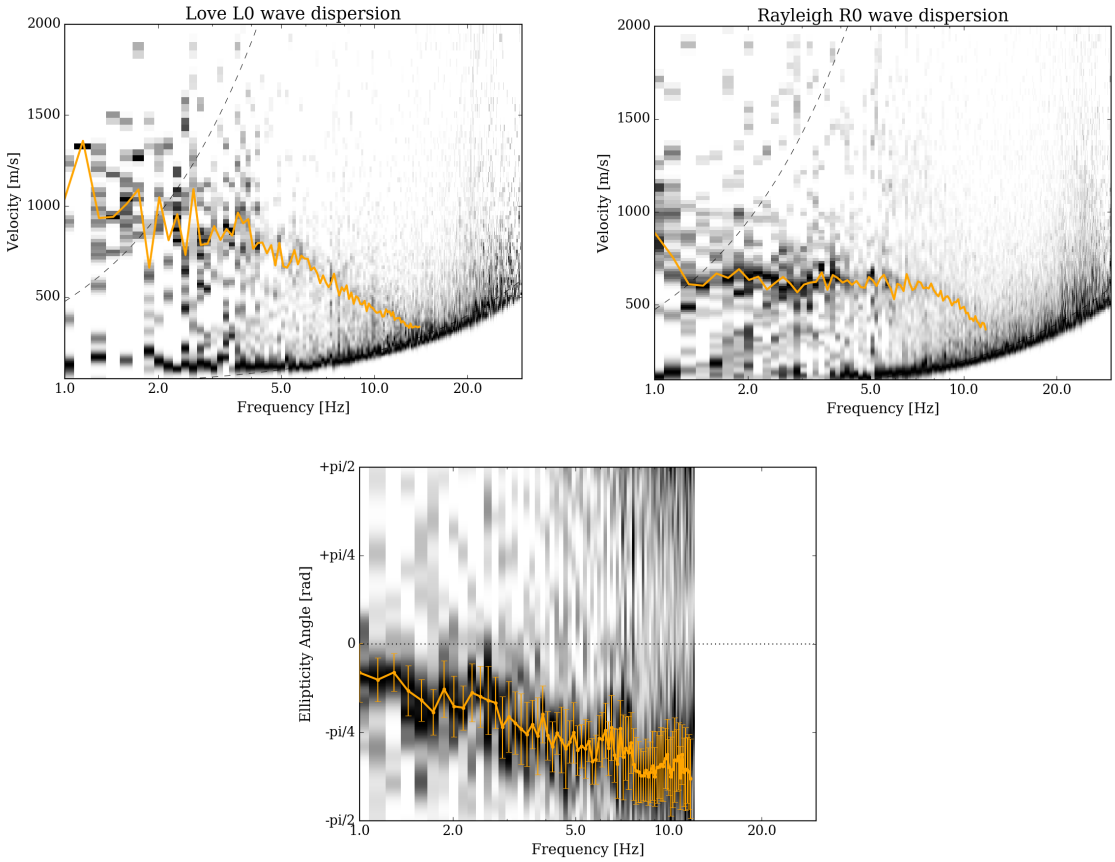


*Figure 10: Dispersion curves for Love and Rayleigh waves (top row) and ellipticity angle curve for Rayleigh waves (bottom row) as obtained with WaveDec (Maranò et al., 2012). The dashed black lines (top rows) represent the array resolution limits, the solid orange line indicates the picked curve and the vertical bars at each frequency show the standard deviation for the ellipticity angle curves.*

## 3.6 Modified SPatial AutoCorrelation

The SPAC (Aki, 1957) curves of the vertical components have been calculated using the MSPAC (Bettig et al., 2001) technique implemented in geopsy (Wathelet et al. 2020). Rings with different radius ranges are defined and for all stations pairs with distances inside this radius range, the cross-correlation is calculated in different frequency ranges. These cross-correlation curves are averaged for all station pairs of the respective ring to give the SPAC curves. The rings are defined in such a way that at least three station pairs contribute and that their connecting vectors have a good directional coverage.

The SPAC Autocorrelation curves are shown in Fig. 11 for all selected rings (central and right columns). The black points indicate the data values which contributed to the final dispersion curve estimation, which was picked using the *spac2disp* function of the geopsy software. A single dispersion curve was picked for the Rayleigh wave between 0.74 and 13.19 Hz as shown by the dark curve in Fig. 11 (left).

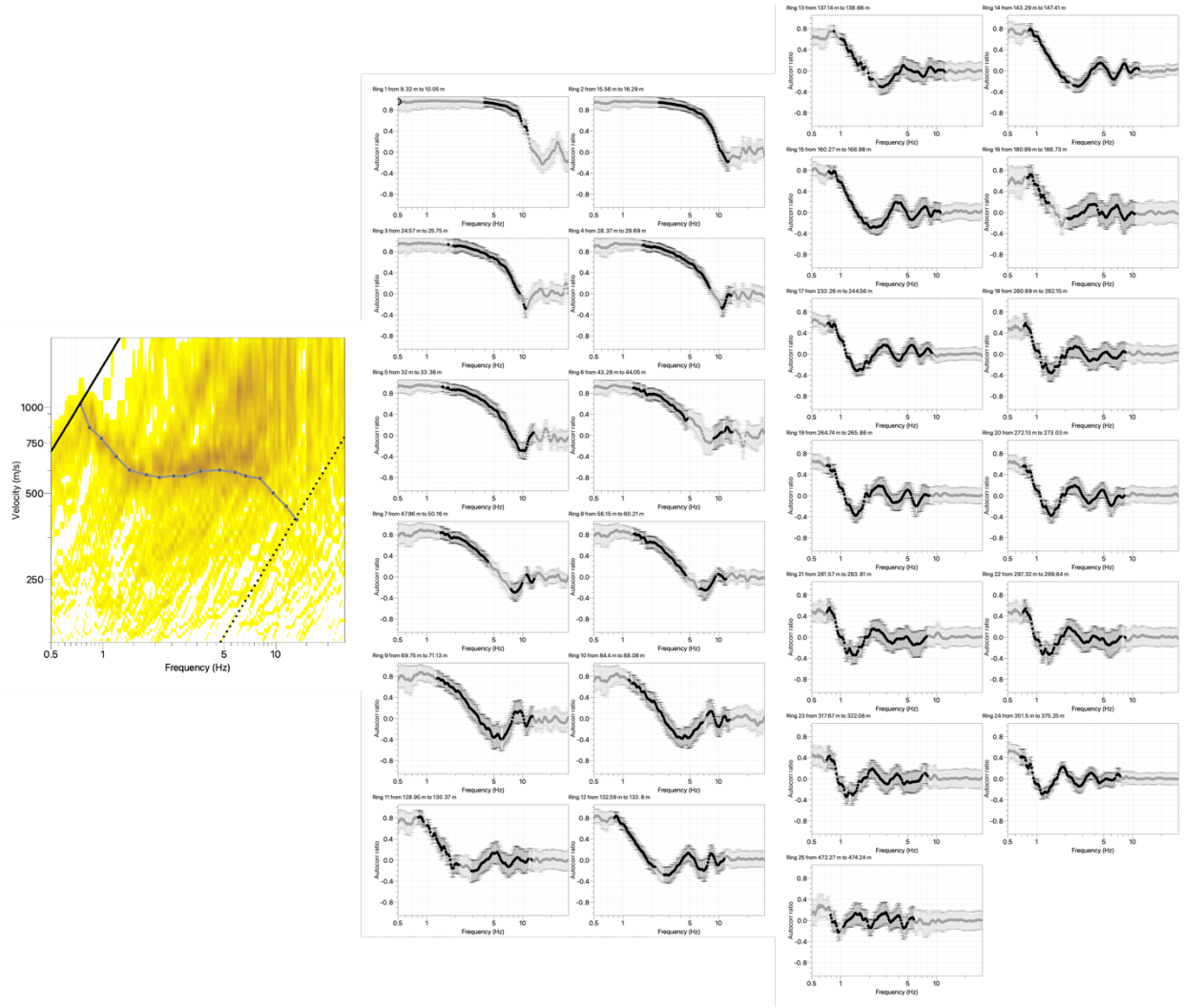


*Figure 11: Rayleigh wave dispersion curve (left) obtained using spac2disp module of geopsy and autocorrelation functions for all rings (center and right). The solid gray line represents the picked data; the black dashed and dotted lines indicate the array resolution limits.*

## 3.7 Summary

Figure 12 gives an overview of the Love and Rayleigh wave dispersion (left and central plots, respectively) and of the Rayleigh wave ellipticity curves (right plot) determined using different approaches. For Love waves, WaveDec and HRFK techniques produce one dispersion curve each; the two curves have similar shapes and velocities over the entire frequency range. The Rayleigh waves were picked using 3C-HRFK (vertical and radial components), WaveDec and MSPAC techniques. The modes at low velocity for the vertical and the radial components of 3C-HRFK and the mode of WaveDec and MSPAC perfectly overlap over the entire frequency range. The two modes at high velocity for the vertical and radial components of 3C-HRFK are straight and also overlap. The dispersion curves shown in Fig. 12 are interpreted as follow: the curves picked for the Love waves are interpreted as the fundamental mode, while the curves at low velocity for the

Rayleigh waves are interpreted as the fundamental mode. To the curve at high velocity, instead, no mode attribution is given.
The ellipticity curves retrieved using the different methods are shown in Fig. 12 (right plot). The RayDec curve is shown for the center of the array (SIOH74) and shows a peak at 0.44 Hz and a trough at 0.85 Hz. After the trough, a second and wider peak is seen at about 8.4 Hz. The ellipticity curves picked using the vertical and the radial components of 3C-HRFK show similar shapes but different amplitude values. The radial curves are shifted upwards when compared with the vertical ones fitting better the RayDec curve. The WaveDec ellipticity curve is picked between 1 and 11.74 Hz and show a huge scatter over the entire frequency range. The curve, picked as ellipticity angle and here converted to ellipticity curve, looks almost straight and crosses all the other curves. The interpretation of the fundamental mode of Rayleigh wave ellipticity curve is provided in the next paragraphs.

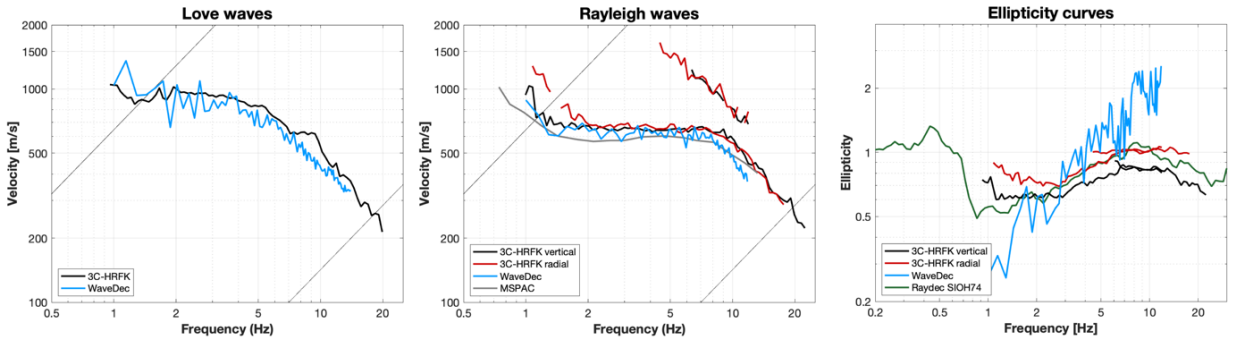


*Figure 12: Comparison between the computed Love (left) and Rayleigh (center) wave dispersion curves and ellipticity curves (right).*

# 4 Data inversion

## 4.1 Inversion targets

We performed four preliminary inversions combining the information of the picked dispersion curves and ellipticity angle curves. These tests were aimed at finding the correct mode attribution and perform the inversion using as much information as possible. The first inversion was performed using the dispersion curves only: one for the Rayleigh waves (0.95-21.60 Hz) and one for the Love waves (1-19.59 Hz). Both dispersion curves were interpreted as fundamental modes and their interpretation doesn't change for all four inversions. The other three inversions differ for the portion of ellipticity angle curve used. In the first case the ellipticity angle curve has negative values corresponding to a retrograde particle motion and consists in two segments: 0.2-0.44 Hz and 1-18.66 Hz. Both curves were picked using the RayDec technique for the SIOH74 station. The second inversion combines the ellipticity angle curves previously mentioned with a new portion of curve picked using RayDec technique. This has positive ellipticity values and stretches from 0.46 to 0.86 Hz. This segment shows a change in the particle motion when compared with the other portions at low and high frequency, corresponding to a change in the particle motion from retrograde to prograde and back to retrograde. The last inversion presents only negative values for the ellipticity angle and consists in a first portion which goes from 0.2 to 0.86 Hz and in a second one between 1.21 and 18.68 Hz. Both segments are picked using the RayDec technique for the SIOH74 seismic station.

Among the four performed inversions, we choose the curves defined in the second inversion for further investigations and show the inverted curves in Fig. 13. From left to right, the fundamental mode of Love waves, the fundamental mode of Rayleigh waves and the fundamental mode for the ellipticity curve (SIOH74) are shown.

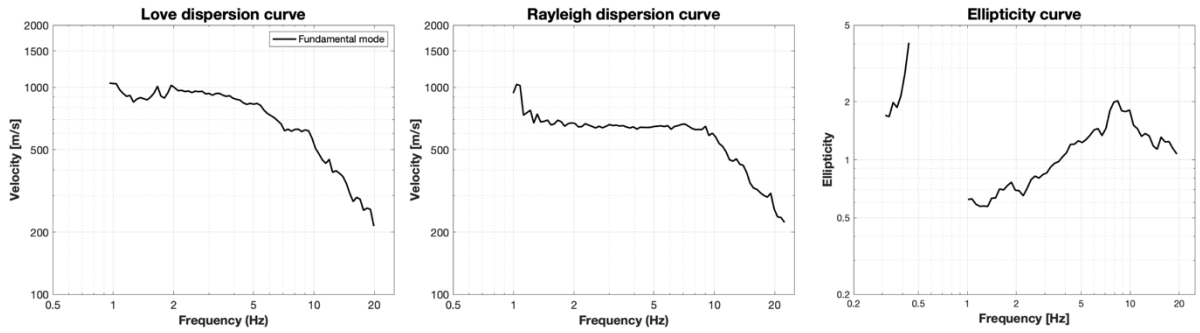


*Figure 13: Overview of the dispersion curves used as target for the different inversions.*

*Table 1: List of the curves used as target in the inversion.*

| Method | Wave type | Mode | Curve type | Frequency range [Hz] |
|---|---|---|---|---|
| 3C-HRFK | Love | fundamental | dispersion | 0.96-19.84 |
| 3C-HRFK | Rayleigh | fundamental | dispersion | 0.92-22.33 |
| RayDec (SIOH74) | Rayleigh | fundamental | ellipticity | 0.2-0.46 & 1-18.65 |

## 4.2 Inversion parameterization

For the inversion, five different parameterizations were tested changing the number of layers over the half-space, from a minimum of six up to twelve. The first four inversions involve free values of thickness and seismic velocities. The S- and P-wave velocities are allowed to range from 50 to 3500 m/s and from 100 to 7500 m/s, respectively. The deepest layer was allowed to range to a depth of 750 m for all parameterizations; the density was fixed to 2300 kg/m$^3$ for the bedrock layer and to 2000 kg/m$^3$ for all the other layers. The last parametrization had layers with fixed thicknesses and consists of 21 layers over the half-space, with the deepest interface at 700 m depth. Equal ranges were defined for the P- and S-wave velocities, while the density is fix to 2000 kg/m$^3$ in the first twelve layers and gradually increase to 2500 kg/m$^3$ at the half-space. In all parametrizations, the velocity inversion was allowed in the shallowest layers down to a maximum depth of 100 meters.

## 4.3 Inversion results

We performed 5 inversions with different parameterizations (see Table 2) using the Dinver routine (http://www.geopsy.org/). Each inversion run produced 280000 models in totals in order to assure a good convergence of the solution. The results of these inversions are shown in Figs. 14 – 18.

*Table 2: List of inversions*

| Inversion | Number of layers | Number of models | Minimum misfit |
|---|---|---|---|
| SIOH 7l | 7 | 280000 | 0.583 |
| SIOH 9l | 9 | 280000 | 0.519 |
| SIOH 11l | 11 | 280000 | 0.607 |
| SIOH 13l | 13 | 280000 | 0.649 |
| SIOH fix | 21 | 280000 | 0.661 |

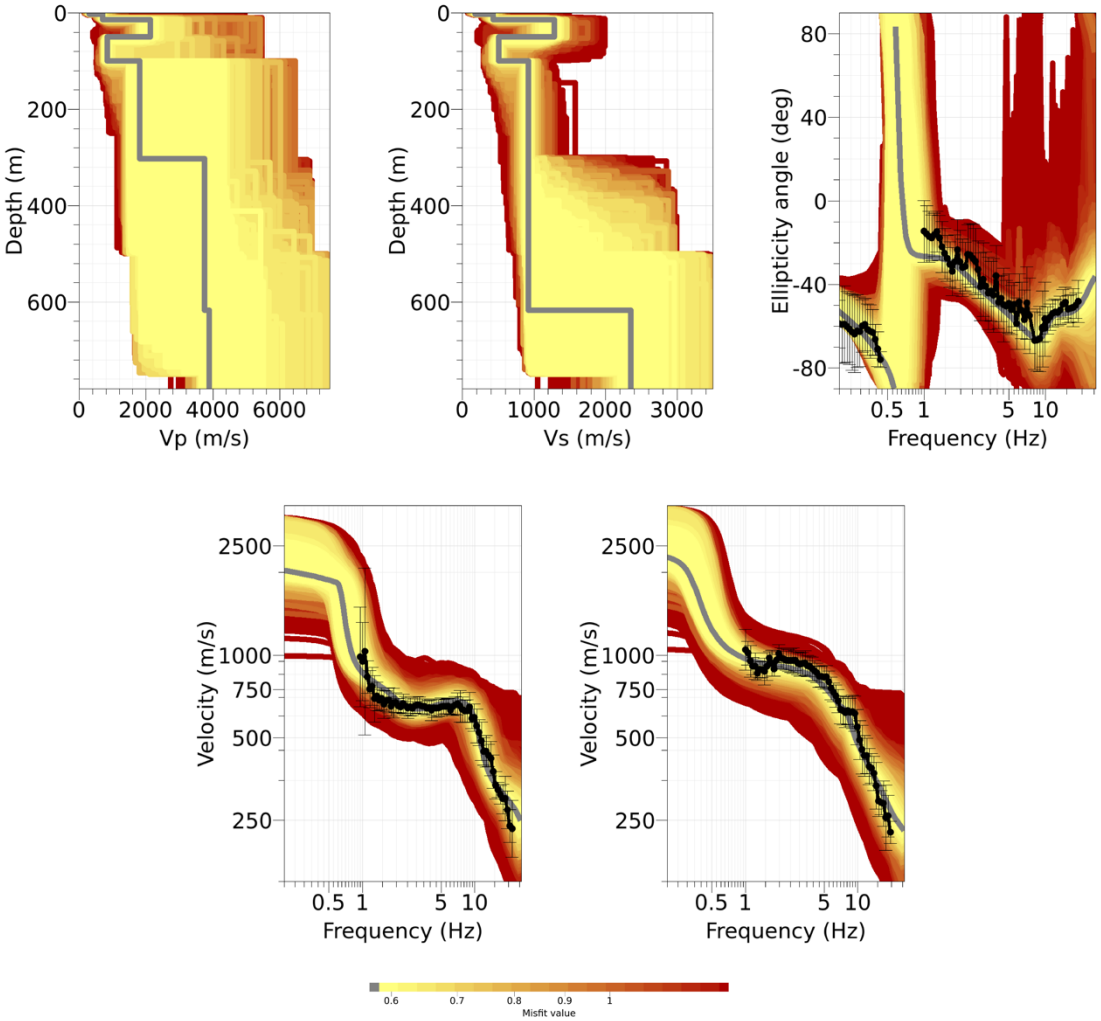


*Figure 14: Inversion* SIOH *7l. Top line: P-wave velocity profiles (left), S-wave velocity profiles (center) and Ellipticity angle curve (right). Bottom line: Dispersion curves for the fundamental mode of Rayleigh waves (left) and fundamental mode of Love waves (right). The black dots indicate the data points used for the inversion, the black bars the standard deviation of the inverted curve, while the gray line shows the best-fitting model.*

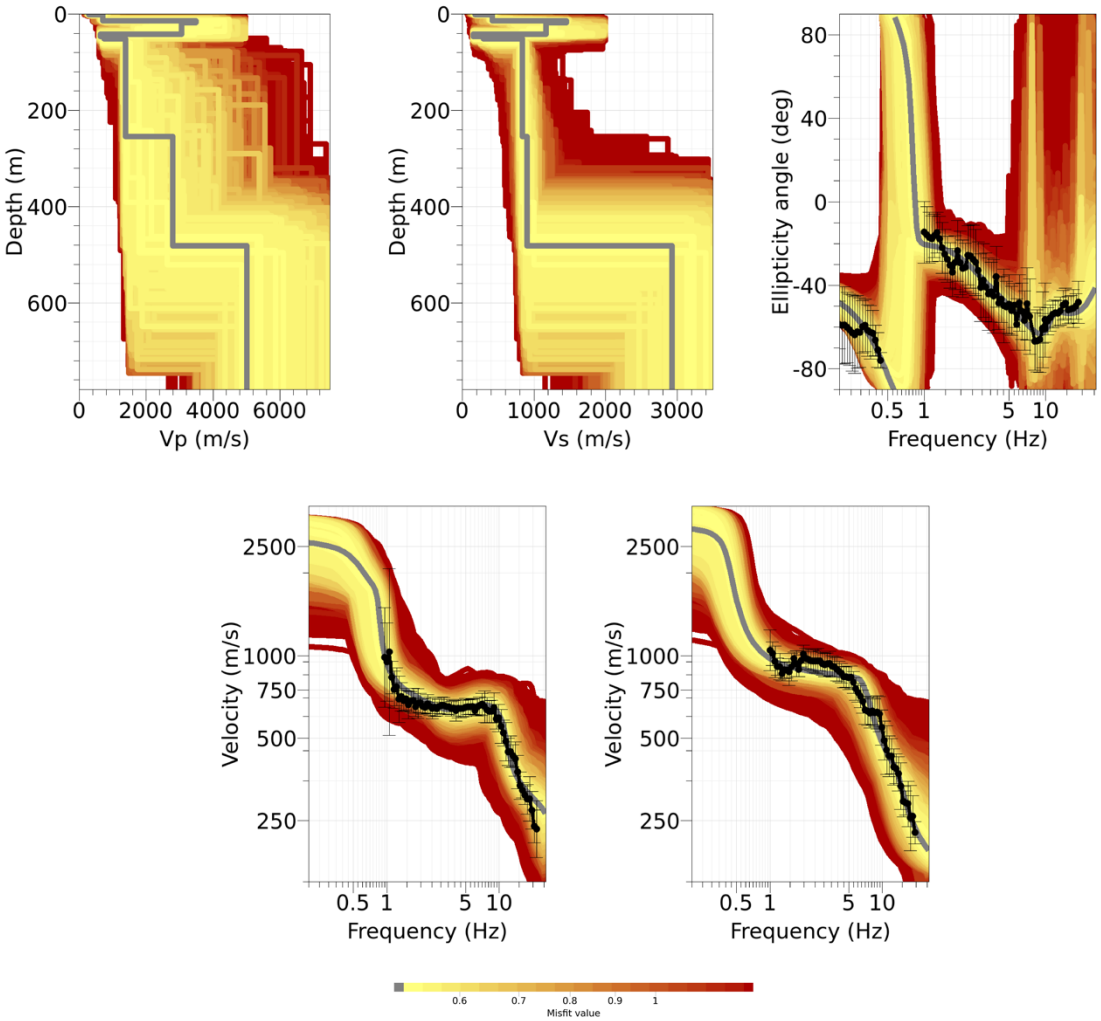


*Figure 15: Inversion* SIOH *9l. Top line: P-wave velocity profiles (left), S-wave velocity profiles (center) and Ellipticity angle curve (right). Bottom line: Dispersion curves for the fundamental mode of Rayleigh waves (left) and fundamental mode of Love waves (right). The black dots indicate the data points used for the inversion, the black bars the standard deviation of the inverted curve, while the gray line shows the best-fitting model.*

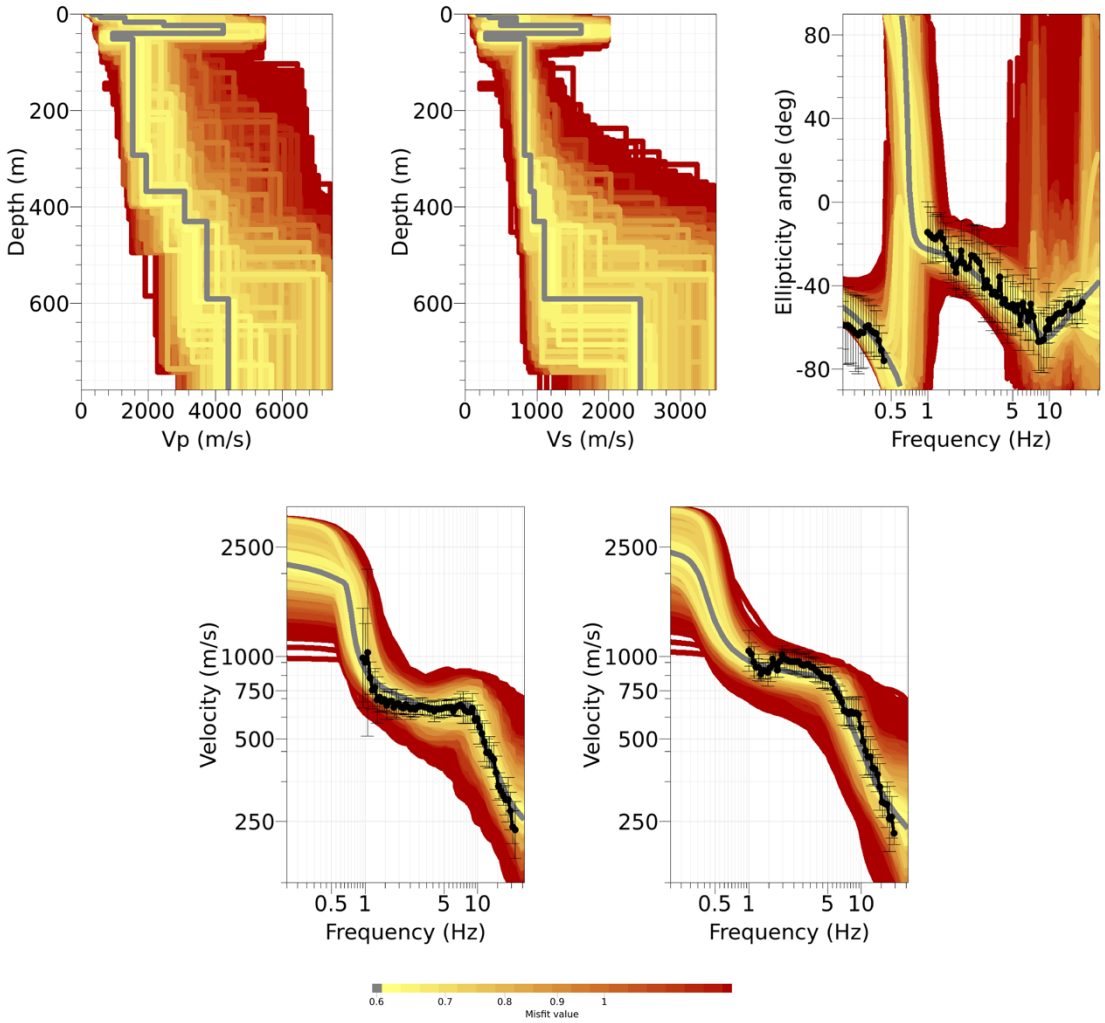


*Figure 16: Inversion* SIOH *11l. Top line: P-wave velocity profiles (left), S-wave velocity profiles (center) and Ellipticity angle curve (right). Bottom line: Dispersion curves for the fundamental mode of Rayleigh waves (left) and fundamental mode of Love waves (right). The black dots indicate the data points used for the inversion, the black bars the standard deviation of the inverted curve, while the gray line shows the best-fitting model.*

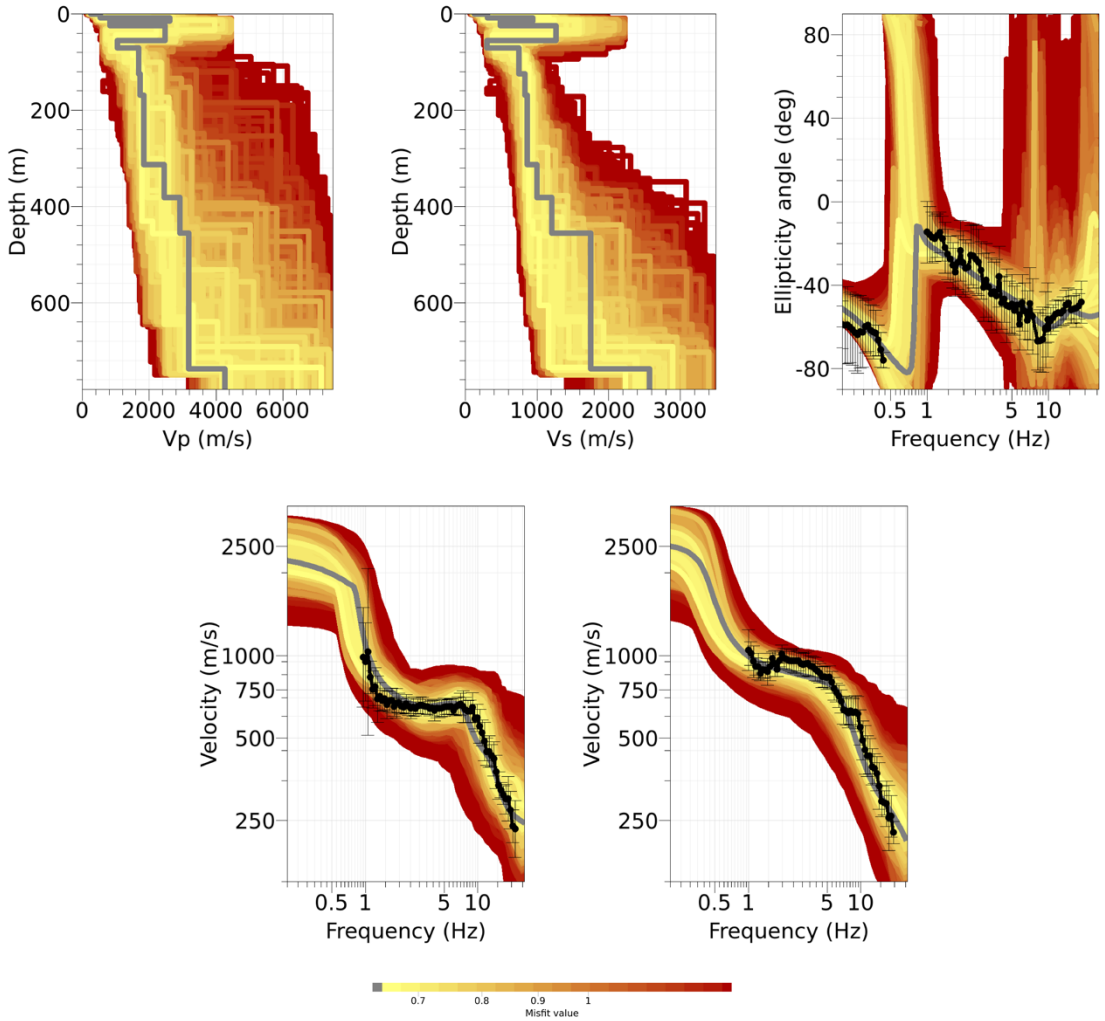


*Figure 17: Inversion* SIOH *13l. Top line: P-wave velocity profiles (left), S-wave velocity profiles (center) and Ellipticity angle curve (right). Bottom line: Dispersion curves for the fundamental mode of Rayleigh waves (left) and fundamental mode of Love waves (right). The black dots indicate the data points used for the inversion, the black bars the standard deviation of the inverted curve, while the gray line shows the best-fitting model.*

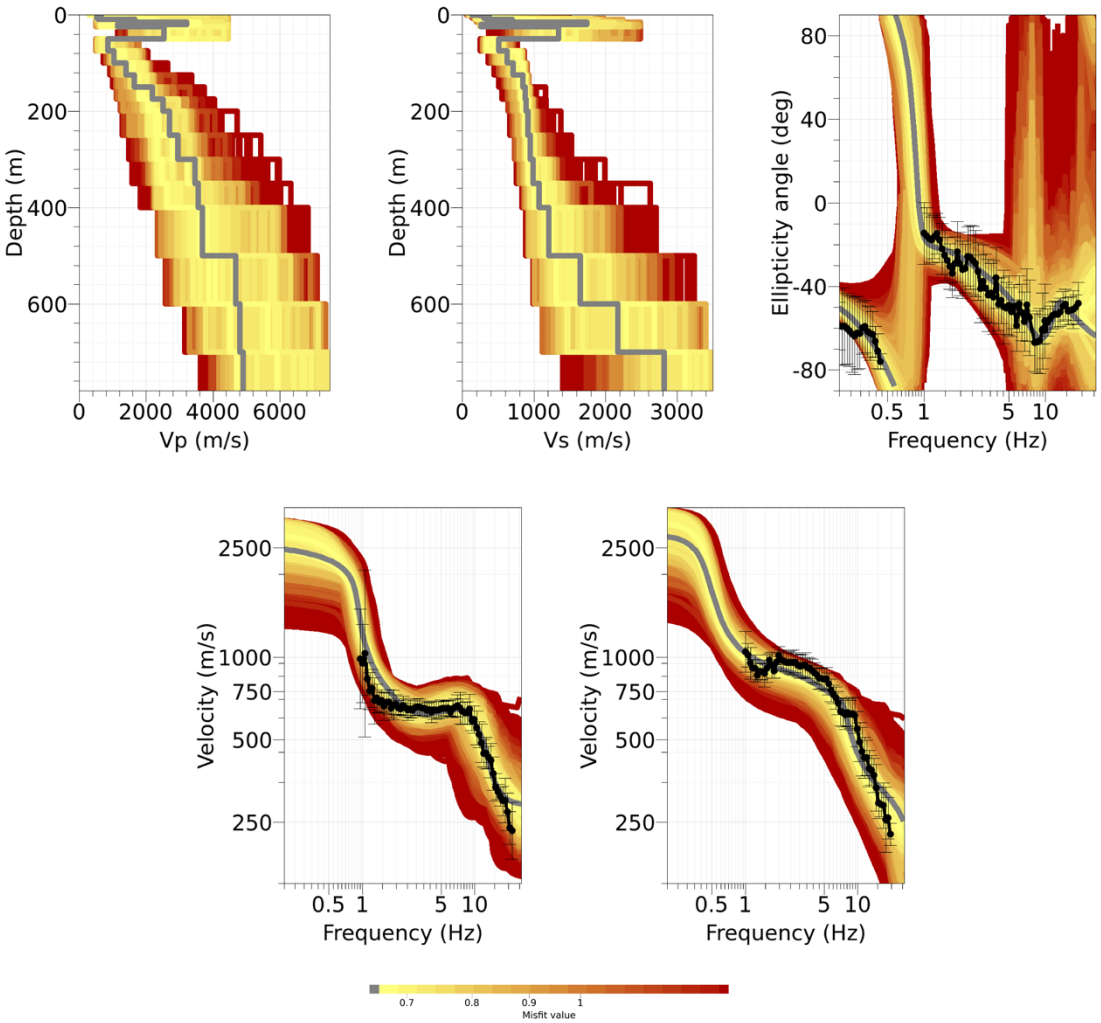


*Figure 18: Inversion* SIOH *fix. Top line: P-wave velocity profiles (left), S-wave velocity profiles (center) and Ellipticity angle curve (right). Bottom line: Dispersion curves for the fundamental mode of Rayleigh waves (left) and fundamental mode of Love waves (right). The black dots indicate the data points used for the inversion, the black bars the standard deviation of the inverted curve, while the gray line shows the best-fitting model.*

## 4.4 Inversion results - Neopsy

In addition to the five inversions performed using the dinver routine, two inversions were performed using the multizonal transdimentional Bayesian formulation (Neopsy – Hallo et al. 2021). The targets of both inversions are the fundamental modes of Rayleigh (0.92-22.33 Hz) and Love (0.96-19.84 Hz) waves dispersion curves which were combined with the ellipticity curves information (0.31-0.44 Hz and 1.07-24.21 Hz). In the first inversion we run Neopsy using the fundamental mode of Rayleigh wave ellipticity angle curve, while in the second one we use the ellipticity curve computed using RayDec technique over the same frequency range. This choice is aimed at exploring the performances of Neopsy using different information for the ellipticity and compare the final results. The parametrization chosen for the seismic velocities, density, Poisson's ratio and depth is defined within ranges: the S- and P-wave velocities range from 50 to 4000 m/s and from 100 to 8000 m/s, respectively, the density adjusts between 2000 and 3000 kg/m$^3$, while the Poisson's ratio is set to change between 0.2 and 0.45. The maximum allowed depth is 800 m, while the velocity inversion is set to a depth of 100 m. The inversion produced 5000 initial models and 25000 new models for a total of 30000 models.

The results of the inversion are shown in Figs. 19 and 21 for the ellipticity angle curve and the ellipticity curve, respectively. The corresponding posterior marginal Probability Density Functions (PDF) and the resulting profiles for $v_p$, $v_s$, $\rho$ and $\upsilon$ are shown in Figs. 20 and 22, respectively. The blue profile shows the results for the best model using the Maximum Likelihood (ML) method, while the magenta color represents the model with the Maximum A Posteriori (MAP) probability.

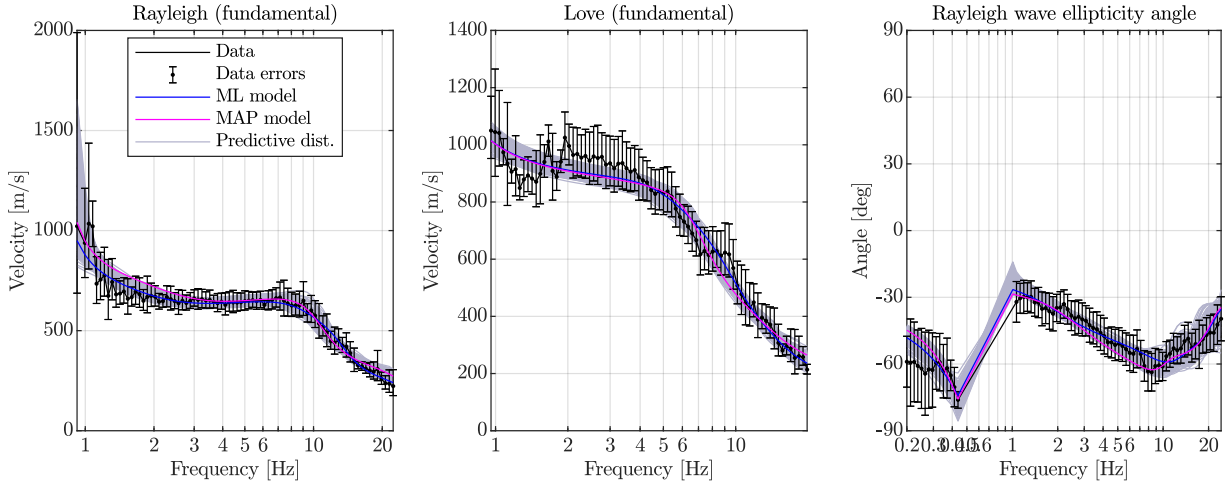


*Figure 19: Results for the inversion using multizonal transdimensional Bayesian formulation. From left to right: Rayleigh wave fundamental mode, Love wave fundamental mode and Rayleigh wave ellipticity curve.*

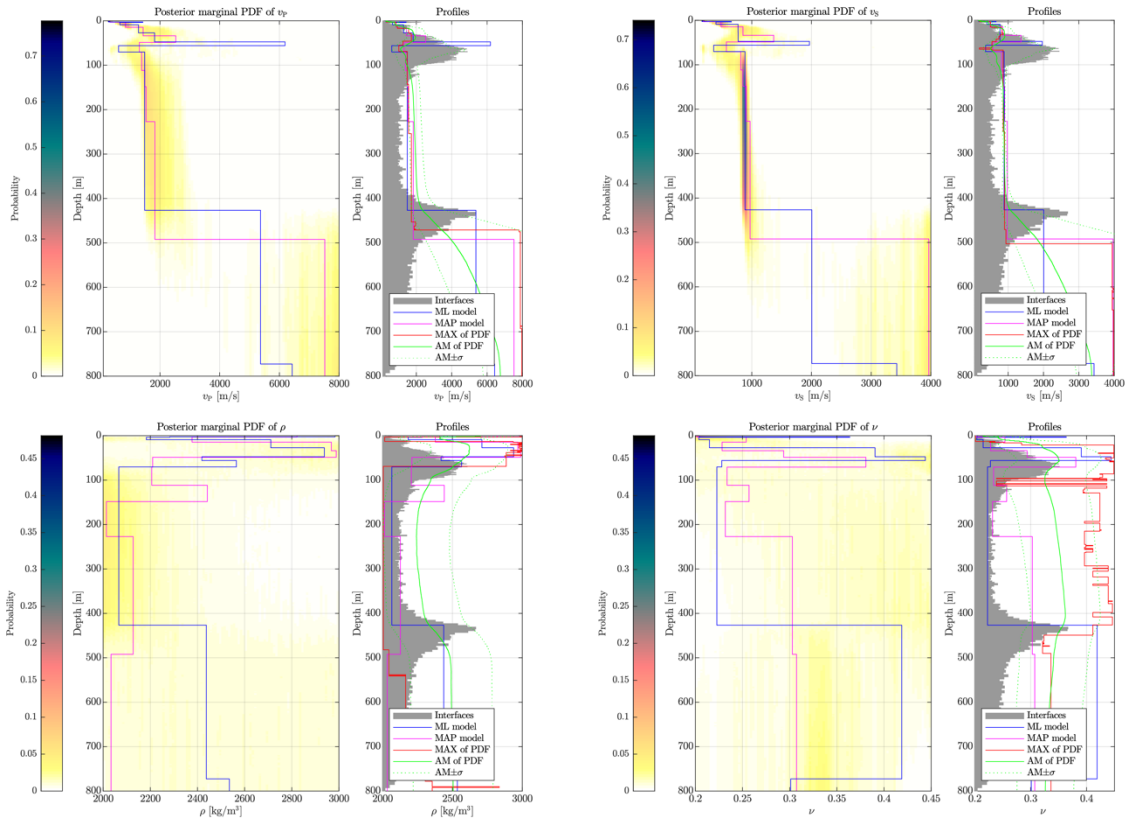


*Figure 20: Posterior marginal PDF and profiles of P-waves (top left), S-waves (top right), density (bottom left) and Poisson's ratio (bottom right). Overview of the best profiles for each PDF for the Maximum Likelihood model (ML - blue) and the Maximum A Posteriori model (MAP - magenta).*

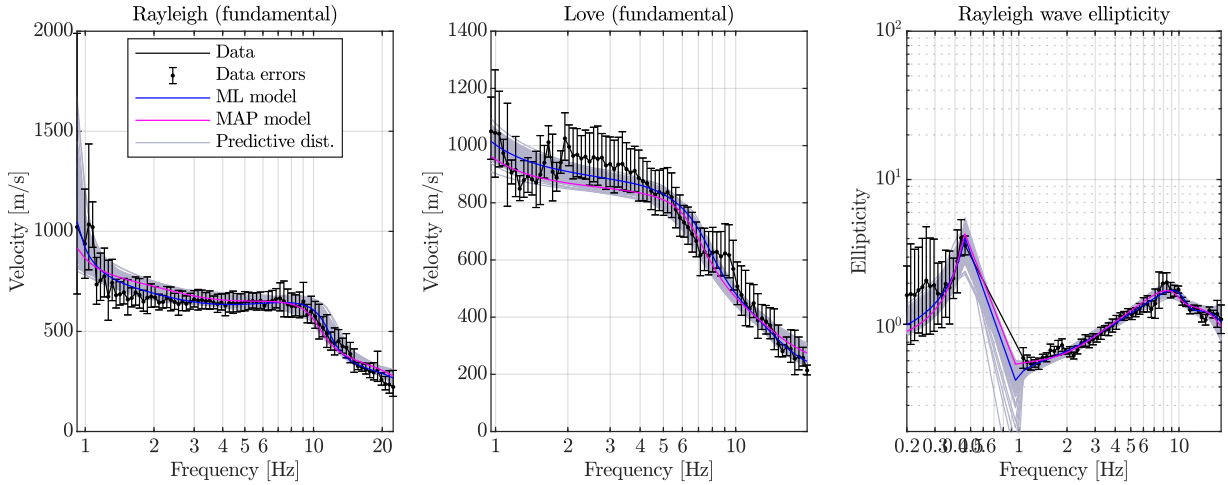


*Figure 21: Results for the inversion using multizonal transdimensional Bayesian formulation. From left to right: Rayleigh wave fundamental mode, Love wave fundamental mode and Rayleigh wave ellipticity angle curve.*

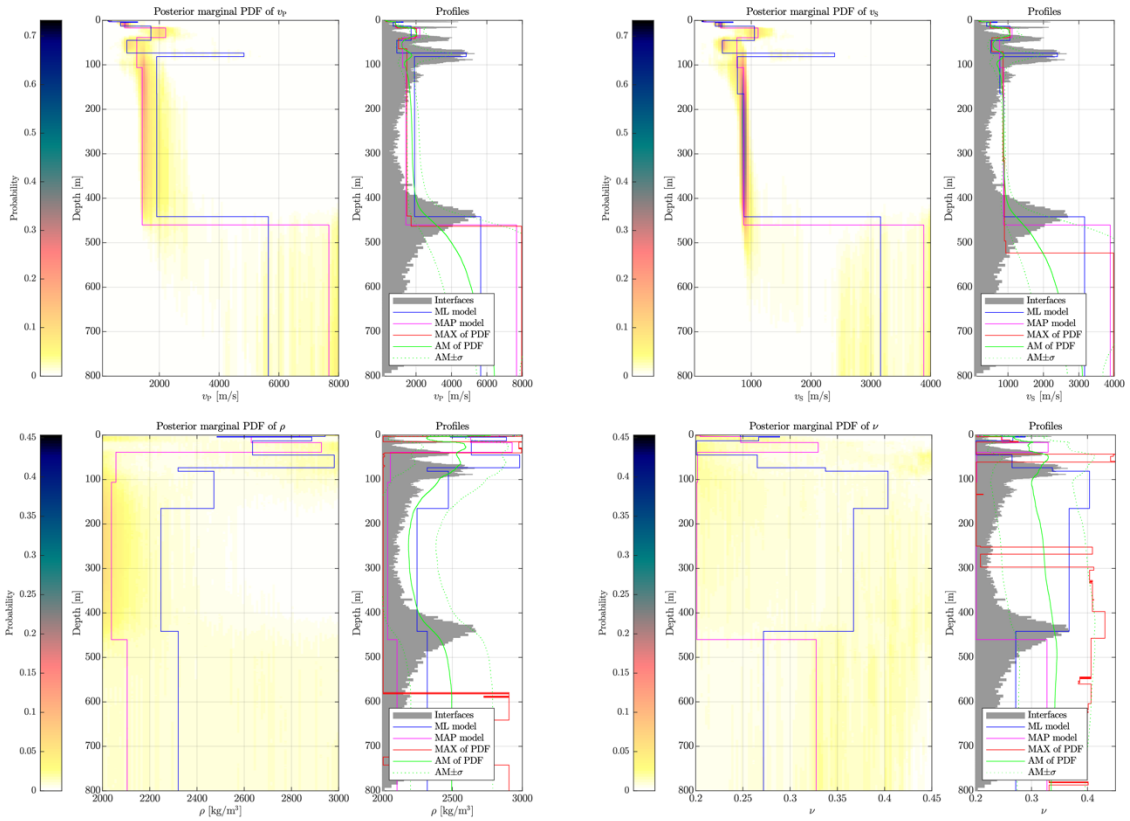


*Figure 22: Posterior marginal PDF and profiles of P-waves (top left), S-waves (top right), density (bottom left) and Poisson's ratio (bottom right). Overview of the best profiles for each PDF for the Maximum Likelihood model (ML - blue) and the Maximum A Posteriori model (MAP - magenta).*

## 4.5 Discussion of the inversion results

The best-fitting models from each inversion are shown in Fig. 23. These correspond to the S-wave velocity profiles with the lowest misfit among all the runs performed using *dinver* and Neopsy. The results of *dinver* are shown in green and gray colors, while the ML and MAP profiles from Neopsy are shown in blue and magenta, respectively.

In the first 30 meters, the *dinver* velocity profiles (*SIOH7l* and *SIOH9l*) show two interfaces at about 2 and 14.1 m. The *SIOH9l* model, after the second interface, presents a velocity inversion down to 42 m with S-wave velocities of 1167 m/s. A similar pattern consisting of two interfaces and a velocity inversion can be seen for the velocity models *SIOH11l* and *SIOH13l*. While the first interface is in agreement with the depth found for the velocity profiles *SIOH7l* and *SIOH9l*, the second interface is shallower and located at about 8.5 m. The velocity inversion starts at 17.3 m for *SIOH11l* velocity model and at 15.4 m for *SIOH13l*. For both cases the inversion ends at about 25 meters depth. The fix layers velocity profile (*SIOHfix*) shows three interfaces at 2, 10 and 15 meters. Below these interfaces a velocity inversion is found and the S-wave velocity values decrease to 262 m/s. The end of the velocity inversion layer is in agreement with the results found for *SIOH11l* and *SIOH13l*.

The results for Neopsy are shown using the ellipticity angle curve (dashed lines) and the ellipticity curves (solid lines). The MAP and the ML models for the ellipticity angle curve show two

interfaces in the shallowest 30 meters: at about 3 and 14.6 m (MAP model) and at about 2.6 m and 8.9 m (ML model). While the first interface is similar and in agreement with the results of all the other velocity models, the second interface has different depths and it is in agreement with *SIOH11l* and *SIOH13l* only. In the ML model, between the two interfaces, a velocity inversion with S-wave velocity down to 399 m/s takes place. The MAP model, instead, shows a gradient.
The MAP model resulting from the inversion of the ellipticity curve shows one interface at 3.4 m and the other at 17 m, similar to *SIOH7l* and *SIOH9l* models. The ML model for the same inversion presents a thin layer of 1.5 m with a strong velocity contrast (Vs = 695 m/s) followed by a velocity inversion between 4.6 and 13 meters.
Between 30 and 100 m, all velocity profiles show one additional velocity inversion. *SIOH9l* and *SIOH11l* present an inversion between 40 and 51 m, a bit shallower if compared with the velocity inversion for *SIOH13l* which is located between 55 and 70 m. The velocity inversion in *SIOH7l* stretches between 50 and 100 m and shows similarity with the *SIOHfix* velocity profile.
The velocity inversion in the MAP model for the ellipticity angle curve shows a layer of about 15 m and S-wave velocity of 1367 m/s which is followed by a velocity inversion where the S-wave velocity decreases to 575 m/s. The ML model, instead, presents a thin layer at 47.5 m with S-wave velocity of 1967 m/s below which a velocity inversion takes place down to 70 m. Also the MAP model using the ellipticity curve as input shows a wide velocity inversion extending from 38.7 to 106 meters with S-wave of 761 m/s. The ML model, instead, in addition to a velocity inversion presents a strong velocity contrast with S-wave velocities up to 2394 m/s, between 73.5 and 81.4 m.
The depth of the half-space shows two trends: the MAP model for Neopsy using the ellipticity angle curve, the MAP and ML models using the ellipticity curve and the *SIOH7l* model from *dinver* inversion show a strong velocity contrast with S-wave velocities up to 3967 m/s at depths of 441-492 meters. The remaining 4 profiles from *dinver* inversion and the ML model from the inversion using the ellipticity angle curve show a deeper half-space with seismic velocities increasing with depth following a gradient. The depth of the half-space is at about 772 m for the ML model using the ellipticity curve, at 600 meters for *SIOH9l* and *SIOH11l* models and at 738 m for *SIOH13l*. The fix layer profile (*SIOHfix*) has the half-space at 700 m with S-wave velocities of 2818 m/s. Among the *dinver* results, the *SIOH7l* velocity profile has low resolution in the deep subsurface, resulting in a strong velocity contrast for the half-space and it was not used for the calculation of the SH-wave transfer function.
The velocity profiles resulting from the different inversions have $V_{S30}$ ranging between 442.0 and 557.0 m/s, with an average value of 504.5 ± 51.9 m/s. The Neopsy models using the ellipticity angle have $V_{S30}$ of 518.5 for the MAP model and 517.8 m/s for the ML model. Similar values were found for the Neopsy inversion using the ellipticity curve as input ($V_{S30}$ ML = 528.2 m/s; $V_{S30}$ MAP = 534.5 m/s).

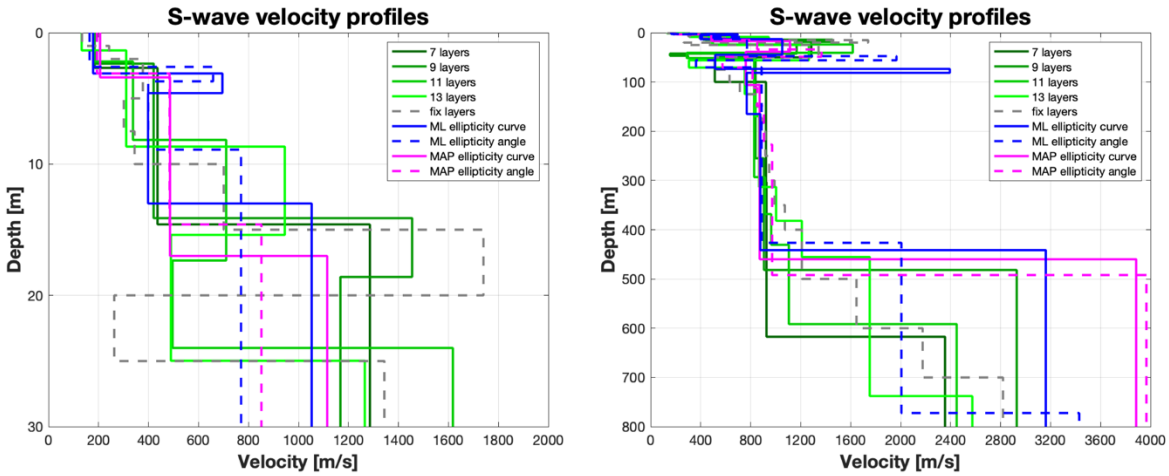


*Figure 23: Overview of the best shear-wave velocity profiles of the different inversions (left) and zoom on the upper 30 m of the inversion profiles.*

# 5 Further results from the inverted profiles

## 5.1 SH transfer function

In Figure 24, the average theoretical shear-wave transfer function for the best models of four tested parametrizations (*SIOH9l*, *SIOH11l*, *SIOH13l* and *SIOHfix*) and the empirical amplification function for SIOH station is shown. As of today (16.06.2022), the SIOH station has a maximum number of 4 earthquakes in the frequency range 0.58-7.32 Hz, decreasing to zero at 11.10 Hz.
The SH-wave transfer function in black and gray colors has a minimum amplification of 0.59 at 15.5 Hz increasing to 7.65 at 22.99 Hz. The curve appears rather flat over the entire frequency range with mild peaks at 0.43 and 1.13 Hz. An increase in the standard deviation values can be seen above 9.37 Hz. A sharp and tall peak takes place at 23.03 Hz.
The empirical amplification function in red shows a good fit with the SH-wave transfer function in terms of amplification values and shape, over the entire frequency range. This agreement occurs between 0.5 and 7.2 Hz; at higher frequencies similar values can be seen for what concerns the amplification values but not the shape. The SH-wave transfer functions of MAP and ML models present several peaks becoming sharper and higher towards high frequency. The general shape of the SH-wave transfer function from Neopsy do not replicate the shape of the empirical amplification function but have comparable amplification values over the entire frequency range.

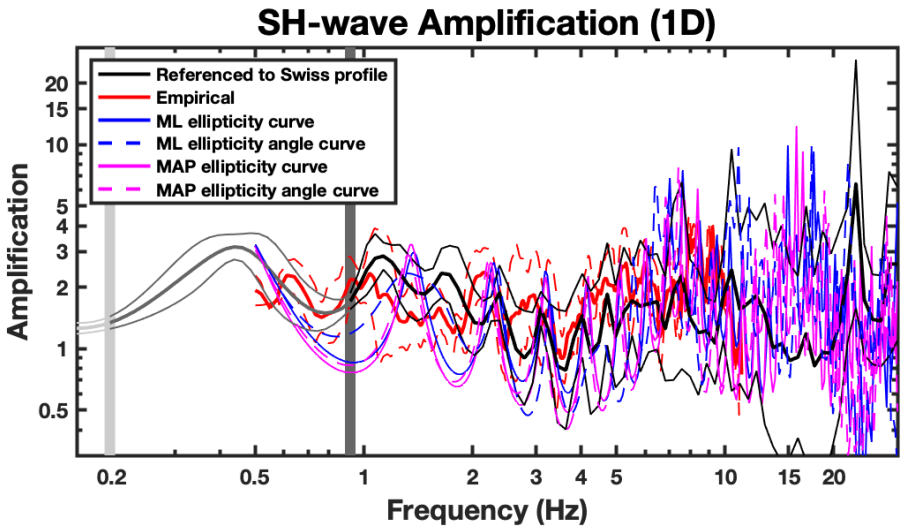


*Figure 24: Modeled amplification function and standard deviation using the best dinver velocity profiles (black lines), the best Maximum A Posteriori models (magenta lines) and the best Maximum Likelihood models (blue lines)*. In red the empirical amplification function and its standard deviation for SIOH station.

## 5.2 Quarter-wavelength representation

The quarter-wavelength velocity approach (Joyner et al., 1981) provides, for a given frequency, the average velocity at a depth corresponding to 1/4 of the wavelength of interest. Figure 25 shows the quarter-wavelength results for the best velocity models of all inversions using the fundamental modes of Rayleigh and Love wave dispersion curves and the Rayleigh wave ellipticity angle. The results using this proxy, considering frequency limits of the experimental data between 0.92 to 22.3 Hz for the dispersion curves and between 0.2 and 18.7 Hz for the ellipticity curves, are well constrained down to 30 m. The dispersion curves provide reliable information down to about 197 m, while the ellipticity curve constraints our model at much higher depths (about 2140 m). The quarter-wavelength impedance contrast introduced by Poggi et al. (2012) is also displayed in Fig. 25. It corresponds to the ratio between two quarter-wavelength average velocities, respectively from the top and the bottom part of the velocity profile, at a given frequency.

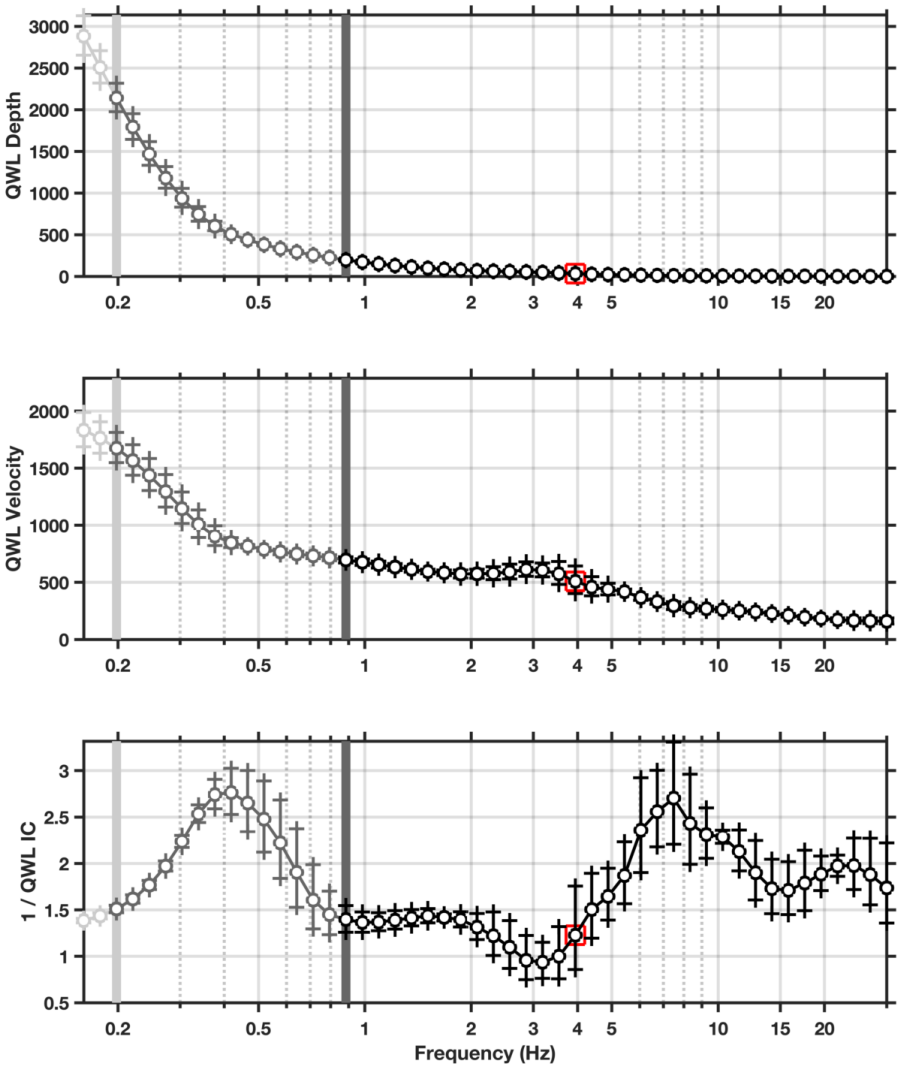


*Figure 25: Quarter wavelength representation of the velocity profiles for the best models of the inversions (top: depth, center: velocity, bottom: impedance contrast). The grey light bar shows ellipticity lower frequency value, dark grey bar indicates lower frequency value obtained with dispersion curves and red square corresponds to $f_{30}$ (frequency related to the depth of 30 m).*

# 6 Discussion and conclusions

The passive array measurement performed in Sion in September 2021 allowed the investigation of the subsurface around the SIOH station.

The H/V analysis pointed out that the study area is generally homogeneous at frequencies below 4 Hz. Two peaks can be distinguished at low (0.45-0.49 Hz) and high frequencies (5.91-8.65 Hz) at almost all sites: the one at low frequency is narrow, sharp and reaches amplitudes of 4. The other is wide and located at lower amplitudes. The interpretation of these two H/V peaks is fundamental mode ($f_0$) and first higher mode ($f_1$), respectively. The $f_0$ peak is visible over the entire study area

and do not show any lateral variability; the $f_1$ peak, instead, is recognized in the center of the array and towards south-west. Due to its areal distribution and based on the geological information, its origin might be linked with the distribution of artificial deposits carried for the construction of Sion hospital. The results of RayDec curves show results similar to the H/V curves (Fig. 5 – right plot).

The inversion of Rayleigh and Love wave dispersion curves and of the Rayleigh wave ellipticity curve is performed using *dinver* and Neopsy techniques. The S-wave velocity profiles estimated in this work investigate the subsurface down to about 800 m. In the shallowest 30 m, most of the velocity profiles show two interfaces at about 2-3 m and at 8 or 15 m. These are divided by one or more velocity inversions taking place at different depths, depending on the velocity profile. *SIOH7l* and the MAP models are the only velocity profiles not showing a velocity inversion in the first 30 meters. At about 100 meters, a third interface can be distinguished in all velocity profiles followed by a rather thick layer with S-wave velocity of about 870 m/s. The depth of the half-space shows two trends: a strong velocity contrast at about 460 m and S-wave velocities up to 3967 m/s (MAP model) and a more gentle gradient with S-wave velocities up to 3428 m/s up to 772 m (ML model). The fix layers velocity profile shows one strong velocity contrast at 15 m followed by a velocity inversion at 20 m. At higher depths no strong velocity contrast can be seen but a gradual velocity increase down to 700 m, where the half-space is located (Vs = 2819 m/s).

The depth of the half-space is not constrained in an univocal way by the different inversions. This is due to the restricted frequency range of the dispersion curves and to the missing information concerning the ellipticity peak for the ellipticity curve.

The average $V_{S30}$ value of the site is 504.55 m/s, corresponding to soil class B in EC8 and SIA261 classifications. The theoretical shear-wave transfer function for the study area predicts a rather flat amplification between 0.15 and 30 Hz with two mild peaks and a sharp peak at 23 Hz. The result shows good agreement in terms of shape and amplitudes with the empirical amplification function measured at SIOH station. The empirical amplification for the SIOH station was computed using a maximum of 4 earthquakes in the frequency range 0.58-7.32 Hz, decreasing to 0 above 11.1 Hz. A longer recording time will probably improve the fit with the SH-wave transfer function at high frequency. The SH-wave transfer functions computed for the MAP and ML models using the ellipticity curve and the ellipticity angle curves show several and narrow peaks with amplification values close to the empirical function but different shapes.

# References


Burjánek, J., Gassner-Stamm, G., Poggi, V., Moore, J. R., and Fäh, D. (2010). Ambient vibration analysis of an unstable mountain slope. Geophys. J. Int., 180:820–828.

Burjánek, J., Moore, J. R., Molina, F. X. Y., and Fäh, D. (2012). Instrumental evidence of normal mode rock slope vibration. Geophys. J. Int., 188:559–569.

Fäh, D., Gardini, D., et al. (2003). Earthquake Cataloque of Switzerland (ECOS) and the related macroseismic database. Eclogae geol. Helv. 96.

Fäh, D., Wathelet, M., Kristekova, M., Havenith, H., Endrun, B., Stamm, G., Poggi, V., Burjanek, J., and Cornou, C. (2009). Using ellipticity information for site characterisation. NERIES deliverable JRA4 D4, available at http://www.neries-eu.org.

Fritsche, S., Fäh, D., Gisler, M., and Giardini, D. (2006). Reconstructing the damage field of the 1855 earthquake inSwitzerland: historical investigations on a well-documented event Geophys. J. Int. (2006)166, 719–731

Hallo, M., Imperatori W., Panzera F. and Fäh, D. (2021). Joint multizonal transdimensional Bayesian inversion of surface wave dispersion and ellipticity curves for local near-surface imaging. Geophys. J. Int., 226, Issue 1, 627-659

Hobiger, M., Bard, P.-Y., Cornou, C., and Le Bihan, N. (2009). Single station determination of Rayleigh wave ellipticity by using the random decrement technique (RayDec). Geophys. Res. Lett., 36.

Maranò, S., Reller, C., Loeliger, H.-A., and Fäh, D. (2012). Seismic waves estimation and wavefield decomposition: Application to ambient vibrations. Geophys. J. Int., 191:175–188.

Poggi, V. and Fäh, D. (2010). Estimating Rayleigh wave particle motion from three component array analysis of ambient vibrations. Geophys. J. Int., 180:251–267.

Poggi, V., Edwards, B., and Fäh, D. (2010). Characterizing the Vertical-to-Horizontal Ratio of Ground Motion at Soft-Sediment Sites. Bulletin of the Seismological Society of America, 102(6): 2741 2756.

Swisstopo, Swiss Federal Office for Topography (2015) Thickness model of unconsolidated deposits map, https://www.swisstopo.admin.ch/en/geodata/geology/models/unconsolidated-deposits.html#documents (last access 12/07/2022)